Journal of Genetics and Genomics 46 (2019) 5–17

Contents lists available at ScienceDirect

Journal of Genetics and Genomics

Journal homepage: www.journals.elsevier.com/journal-of-genetics-and-genomics/

Original research

Drosophila homolog of the intellectual disability-related long-chain acyl-CoA synthetase 4 is required for neuroblast proliferation

Mingyue Jia [a, b, 1], Danqing Meng [a, b, 1], Mo Chen [a, b, 1], Tingting Li [a, b], Yong Q. Zhang [a, b, *], Aiyu Yao [a, *]

[a] State Key Laboratory of Molecular Developmental Biology, Institute of Genetics and Developmental Biology, Chinese Academy of Sciences, Beijing, 100101, China
[b] University of Chinese Academy of Sciences, Beijing, 100049, China

ARTICLE INFO

Article history:
Received 18 October 2018
Accepted 29 October 2018
Available online 26 December 2018

Keywords:
ACSL4
Drosophila
Mushroom body
Neuroblast
Neural stem cell
Premature differentiation

ABSTRACT

Mutations in *long-chain acyl-CoA synthetase 4* (*ACSL4*) are associated with non-syndromic X-linked intellectual disability (ID). However, the neural functions of ACSL4 and how loss of ACSL4 leads to ID remain largely unexplored. We report here that mutations in *Acsl*, the *Drosophila* ortholog of human *ACSL3* and *ACSL4*, result in developmental defects of the mushroom body (MB), the center of olfactory learning and memory. Specifically, *Acsl* mutants show fewer MB neuroblasts (Nbs) due to reduced proliferation activity and premature differentiation. Consistently, these surviving Nbs show reduced expression of cyclin E, a key regulator of the G1- to S-phase cell cycle transition, and nuclear mislocalization of the transcriptional factor Prospero, which is known to repress self-renewal genes and activate differentiating genes. Furthermore, RNA-seq analysis reveals downregulated Nb- and cell-cycle-related genes and upregulated neuronal differentiation genes in *Acsl* mutant Nbs. As *Drosophila* Acsl and human ACSL4 are functionally conserved, our findings provide novel insights into a critical and previously unappreciated role of Acsl in neurogenesis and the pathogenesis of ACSL4-related ID.

1. Introduction

During brain development, neural stem cells proliferate spatially and temporally to generate a large number of diverse neurons and glial cells. They must remain proliferative without becoming tumorigenic, and remain competent to differentiate without actually differentiating; misregulation of neural stem cells can cause microcephaly, megalencephaly, or brain tumor (Sousa-Nunes et al., 2010; Ming and Song, 2011; Homem et al., 2015). How these cells maintain stemness and proliferate is a fundamental question with clinical significance. The *Drosophila* brain provides a powerful model to study the molecular and genetic mechanisms of neural stem cell activity (Tastan and Liu, 2015; An et al., 2017). Neural stem cells in *Drosophila* brain are called neuroblasts (Nbs). The Nbs in the central brain are classified into type I, type II and mushroom body (MB) Nbs according to their location and lineage characteristics (Sousa-Nunes et al., 2010). During neurogenesis, type I and MB Nbs undergo asymmetric cell division to self-renew and generate a series of smaller daughter cells called ganglion mother cells (GMCs), each of which divides only once to produce a pair of post-mitotic neurons or glial cells (Sousa-Nunes et al., 2010). The MBs of the *Drosophila* brain contain densely packed Kenyon cells which take part in distinct cognitive functions (Heisenberg, 2003). Most Nbs in the *Drosophila* brain quit postembryonic neurogenesis by the early pupal stage, but MB Nbs maintain exceptional proliferation activity that persists until the end of the pupal stage (Truman and Bate, 1988; Ito and Hotta, 1992), providing a unique system to study how proliferation of neural stem cells is regulated at distinct developmental stages.

Intellectual disability (ID), estimated to occur in 1% of the general population worldwide, is characterized by deficits in

Abbreviations: ACSL4, long-chain acyl-CoA synthetase 4; APF, after puparium formation; CycE, cyclin E; Dpn, Deadpan; EdU, 5-ethynyl-2′-deoxyuridine; FACS, fluorescence-activated cell sorting; GMC, ganglion mother cell; ID, intellectual disability; MARCM, mosaic analysis with a repressible cell marker; MB, mushroom body; Mira, Miranda; Nb, neuroblast; NSPC, neural stem and progenitor cells; PH3, phosphohistone H3; Pros, Prospero; SEM, standard error of the mean.

* Corresponding authors.
E-mail addresses: yqzhang@genetics.ac.cn (Y.Q. Zhang), ayyao@genetics.ac.cn (A. Yao).

[1] These authors contributed equally to this work.

https://doi.org/10.1016/j.jgg.2018.10.006

intellectual functioning and adaptive behavior (Vissers et al., 2016). ID is classified as non-syndromic and syndromic. 'Non-syndromic' means that the patients only show mental disability, while the syndromic ID is usually accompanied by other phenotypes of physical, neurological or metabolic abnormalities (Ropers and Hamel, 2005; Ropers, 2008). *ACSL4*, which encodes a long-chain-fatty-acid-CoA ligase, is the first lipid metabolism gene shown to be associated with non-syndromic ID (Meloni et al., 2002). To date, multiple mutations in *ACSL4* have been reported in ID patients and these mutations account for 1% of X-linked non-syndromic ID (Meloni et al., 2002; Longo et al., 2003). ACSL4 is highly expressed in the adult cerebellum and hippocampus, which are critical for execution of movements and for learning and memory, respectively (Cao et al., 2000; Meloni et al., 2009). However, how ACSL4 regulates brain development and function remains largely unknown.

Acsl, the *Drosophila* homolog of human ACSL3 and ACSL4, regulates visual wiring and axonal transport of synaptic vesicles (Zhang et al., 2009; Liu et al., 2011). More recently, we found that *Acsl* mutants showed peripheral neuromuscular junction (NMJ) overgrowth that was suppressed by reducing the bone morphogenetic protein (BMP) signaling and the abundance of raft-associated lipids (Liu et al., 2014; Huang et al., 2016). However, it is unclear if Acsl regulates brain development. In the present study, we show that loss of Acsl disrupts MB development. Specifically, Acsl is required for efficient proliferation of MB Nbs in a cell-autonomous manner. Furthermore, multiple lines of evidence by immunostaining, live imaging, and RNA-seq analysis reveal impaired cell cycle progression and premature differentiation of MB Nbs in *Acsl* mutants. Together, our results demonstrate that the lipid-metabolizing Acsl plays a critical and previously unidentified role in Nb proliferation activity. As *Drosophila* Acsl and human ACSL4 are functionally conserved, our findings provide novel insights into the mechanism by which Acsl/ACSL4 regulates Nb activity.

2. Results

2.1. Loss of Acsl disrupts adult MB development

To gain insight into the role of Acsl in brain development, we used the well-characterized *Drosophila* MB as a model system. The adult MB comprises a cell body cluster and five axonal lobes. Of these five lobes, the α and α′ lobes project dorsally, while the γ, β and β′ lobes project medially (Crittenden et al., 1998; Lee et al., 1999). Antibodies against the cell adhesion molecule fasciclin II (FasII) label the MB α/β lobes strongly and the γ lobe weakly in wild-type brains (Crittenden et al., 1998). The γ lobes, as well as α/β lobes, showed similar dimensions in both brain hemispheres (Fig. 1A). As *Acsl* null mutants are lethal before adulthood, we examined MB morphology in *Acsl* hypomorphic mutants $Acsl^{8}/Acsl^{05847}$ and $Acsl^{1}/Acsl^{05847}$ which survived to adults but died within two days after eclosion. In $Acsl^{8}/Acsl^{05847}$ mutant adults, 69% of α/β lobes were much thinner than the wild type, while the remaining brains showed loss of lobes including unilateral and bilateral loss of α or α/β lobes (Fig. 1B and M). In addition, β lobes grew across the midline and fused together in 80% of 45 adult $Acsl^{8}/Acsl^{05847}$ mutant brains examined (Fig. 1B, arrow). $Acsl^{1}/Acsl^{05847}$ combination showed weaker but similar phenotypes (Fig. 1C and M), consistent with the allelic series of $Acsl^{8} > Acsl^{1} > Acsl^{05847}$ as previously documented (Zhang et al., 2009).

To identify cell type-specific requirement of Acsl in MB development, we manipulated *Acsl* expression under the control of different *Gal4* lines. The mutant phenotype was recapitulated when *Acsl* was knocked down by RNAi driven by the *elav-Gal4* which expresses in most Nbs of brain and pan-neurons or *OK107-Gal4* which expresses weakly in MB Nbs but highly in MB neurons, but not by MB neuron-specific *30Y-Gal4* (Fig. 1D–F and M). Consistently, overexpression of *Acsl* by *elav-Gal4* as well as the Nb-specific *insc-Gal4* completely rescued the severe MB phenotype of *Acsl* mutants (Fig. 1G, H and M). However, overexpression of *Acsl* by *OK107-Gal4* only partially rescued the phenotype of *Acsl* mutants, probably because of low level expression of Acsl in MB Nbs (Fig. 1I and M), while *30Y-Gal4*-controlled expression of *Acsl* did not rescue the phenotype of *Acsl* mutants (Fig. 1J and M). Taken together, these results indicate that Acsl acts specifically in Nbs to regulate the formation of MB.

Importantly, ectopic expression of wild-type but not ID-associated mutant human ACSL4 (P375L) with reduced enzymatic activity by *elav-Gal4* restored the mutant phenotypes to wild-type level (Fig. 1K–M), demonstrating functional conservation between *Drosophila* Acsl and human ACSL4.

In addition, we analyzed mutant brains across different developmental stages. As shown by anti-FasII staining of 3rd instar larval brains, γ lobes were smaller and thinner in $Acsl^{8}/Acsl^{05847}$ mutants than wild type (Fig. S1A and E). In the wild-type brains, the vertical α and medial β lobes increased gradually with development (Fig. S1B–D). In contrast, the α/β lobes in $Acsl^{8}/Acsl^{05847}$ mutants were smaller and thinner than wild type and the defects persisted with no apparent deterioration throughout pupal development from 48 h to 96 h after puparium formation (APF; Fig. S1F–H), suggesting a developmental rather than degenerative defects.

To further examine the role of Acsl in the development of different MB lobes, we labeled different types of MB neurons with membrane-associated CD8-GFP under the control of specific Gal4 lines. In addition to disrupted α/β lobes as shown above by anti-FasII staining (Fig. 1), the γ and α′/β′ lobes in $Acsl^{8}/Acsl^{05847}$ mutants were also thinner than wild type (Fig. S2). These data show that Acsl is essential for the formation of all MB lobes.

2.2. Loss of Acsl leads to reduced MB clone size

The size of MB lobes was severely decreased in *Acsl* mutants, suggesting that MB Nbs maybe proliferate at a reduced rate, or are lost during development, or both. To distinguish these scenarios, we employed clonal analyses by mosaic analysis with a repressible cell marker (MARCM) technique to quantify the proliferation capacity of individual MB Nbs through all developmental stages. Four MB Nbs in each brain hemisphere have previously been identified by cell lineage analysis. Each of them gives rise to three subtypes of neurons based on their axonal projection patterns and birth dates; specifically, γ neurons are born from embryos (stage 11) until the mid-3rd instar larval stage, α′/β' neurons are born between the mid-3rd instar larval stage and puparium formation, while α/β neurons are born after puparium formation (Ito et al., 1997; Lee et al., 1999; Kunz et al., 2012). We counted the number of all neurons labeled by mCD8-GFP in MB Nb clones from serial confocal images. Wild-type MB Nb clones induced at the 1st instar larval stage consisted of 450.20 ± 11.76 neurons in the adult brain ($n = 11$) (Fig. 2A), while *Acsl* mutant MB Nb clones exhibited a dramatic reduction in the number of neurons: 16.55 ± 1.60 neurons for $Acsl^{KO}$ ($n = 11$), 23.68 ± 1.14 neurons for $Acsl^{8}$ ($n = 19$), and 26.67 ± 4.19 neurons for $Acsl^{1}$ ($n = 6$) (all $P < 0.001$ for all three mutant alleles compared with wild type; Fig. 2B–D). The progenies of each wild-type MB Nb clone projected their axons into three sets of lobes: γ, α′/β′, and α/β (Fig. 2A′). By contrast, the *Acsl* mutant brains contained only γ neurons born by the mid-3rd instar larval stage but no

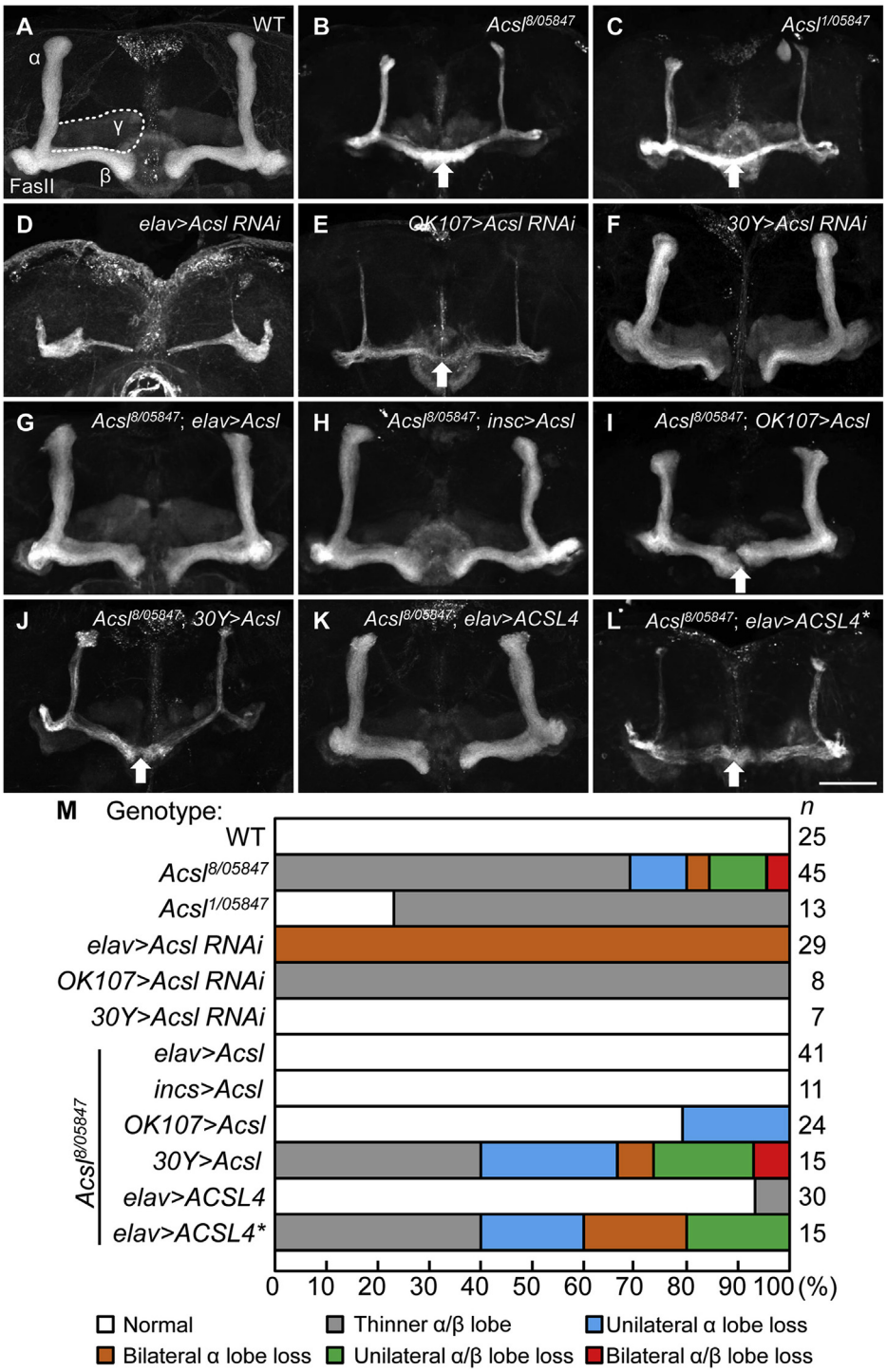

Fig. 1. Acsl is required for normal development of the MB. **A**: In adult wild-type MB, α/β lobes were strongly labeled and γ lobes were weakly labeled (dashed lines) by anti-FasII staining. **B** and **C**: Thinner γ and α/β lobes and fusion of β lobes (arrows) were observed in $Acsl^{8}/Acsl^{05847}$ (**B**) and $Acsl^{1}/Acsl^{05847}$ (**C**) mutants. **D**–**F**: RNAi knockdown of *Acsl* by neural *elav-Gal4* (**D**) and MB-specific *OK107-Gal4* (**E**), but not by pan-MB neuronal *30Y-Gal4* (**F**) caused MB defects. **G**–**J**: The MB defects in $Acsl^{8}/Acsl^{05847}$ mutants were fully rescued by *elav-Gal4*-driven (**G**) and *insc-Gal4*-driven (**H**) expression of *Acsl*, partially rescued by *OK107-Gal4*-driven expression of *Acsl* (**I**), but were not rescued by *30Y-Gal4*-driven expression of *Acsl* (**J**). **K** and **L**: Overexpression of wild-type human *ACSL4* (**K**) but not mutant *ACSL4 (P375L)* (**L**) by *elav-Gal4* largely rescued the $Acsl^{8}/Acsl^{05847}$ mutant phenotype. Scale bars, 50 μm. **M**: Percentages of axonal loss defects in *Acsl* mutants, cell-type specific RNAi knockdowns, and overexpression of *Acsl*, *ACSL4* and *ACSL4 (P375L)* by different Gal4 lines in an $Acsl^{8}/Acsl^{05847}$ mutant background. *ACSL4** indicates *ACSL4 (P375L)*.

α′/β′ and α/β neurons born at later developmental stages (Fig. 2B′–D'). Importantly, overexpression of wild-type *Acsl* or human *ACSL4* fully rescued the reduced number of neurons in $Acsl^{KO}$ mutant clones: 459.30 ± 25.14 cells for $Acsl^{KO}$ + *Acsl* rescue ($n = 4$) and 424 ± 10.92 cells for $Acsl^{KO}$ + *ACSL4* rescue ($n = 4$) ($P > 0.05$ for both rescues compared with wild type; Fig. 2E–F′). These results together support the conclusion that MB Nbs have defects in proliferation, maintenance, or both by the mid-3rd instar larval stage

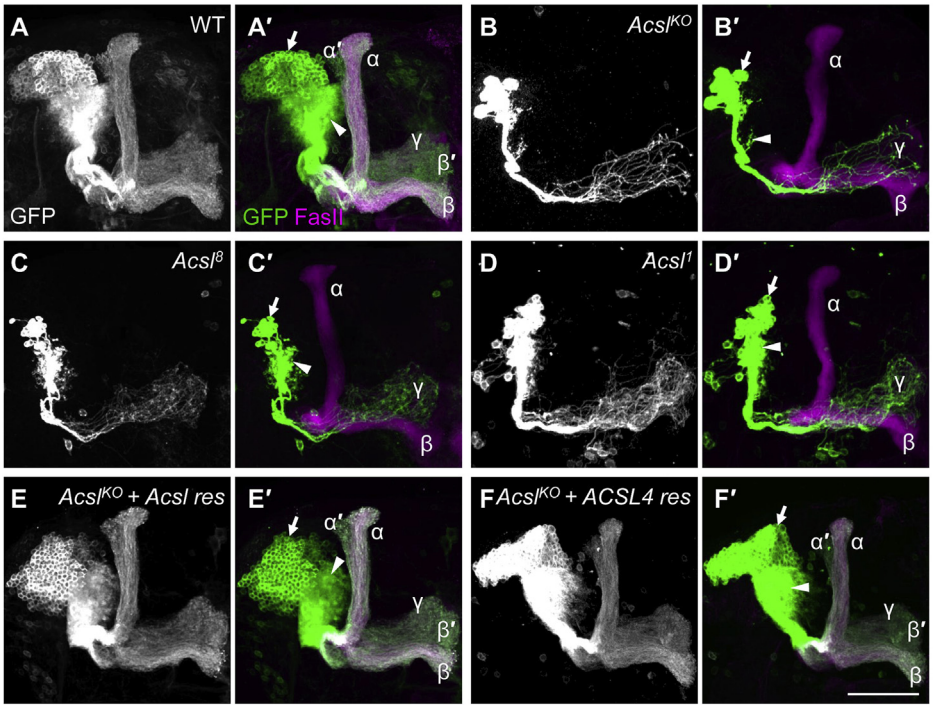

Fig. 2. Acsl regulates Nb clone size. **A** and **A′**: In a single MB Nb clone labeled with mCD8-GFP in wild-type adult brain, three types of MB neurons project their axons into five distinct lobes, α, β, α′, β′, and γ. **B**–**D′**: MB Nb clones of three independent *Acsl* alleles contain fewer Kenyon cells (arrows) and few dendrites (arrowheads). Except for γ neurons, no other types of neurons such as α′/β′ or α/β were generated by the *Acsl* mutant clone. **E**–**F′**: Overexpression of *Acsl* (**E**) and human *ACSL4* (**F**) by *elav-Gal4* in $Acsl^{KO}$ MB Nb clones largely rescued the *Acsl* phenotype, as evidenced by more Kenyon cells, denser calyx and the presence of different lobes compared with the $Acsl^{KO}$ mutant clones. To appropriately display different lobes, the cell body and calyx of MB were overexposured. Scale bars, 50 μm.

in *Acsl* mutants.

The clonal analyses presented above showed that loss of Acsl led to a reduced size of MB clones containing only γ neurons in the adult brain. It was possible that the MB Nbs cease proliferation or are lost by the mid-3rd instar larval stage in *Acsl* mutants. To distinguish between these two possibilities, we quantified Nb number in MB Nb clones in late 3rd instar larval brains. In these clones, Nbs were labeled specifically by Miranda (Mira), which is expressed in the cell cortex at interphase and asymmetrically localizes in the basal cortex during mitosis (Ikeshima-Kataoka et al., 1997; Shen et al., 1997; Homem and Knoblich, 2012). Nb can also be readily recognized by its larger size and weaker GFP labeling compared with its neighboring GMCs and neurons (Fig. 3A–A′′′). In wild-type brains, all 12 MB Nb clones examined contained a single large Nb at the late 3rd instar larval stage (Fig. 3A, A′ and D). In contrast, the percentage of clones with Nbs was significantly decreased in *Acsl* mutant MB Nb clones, i.e., only 3 Nbs in 12 $Acsl^{KO}$ clones and 1 Nb in 20 $Acsl^{1}$ clones (Fig. 3B, B′, C, C′ and D). Furthermore, antibody staining against the mitotic M-phase marker phosphohistone H3 (PH3) revealed that 4/12 single MB Nb clones were positive for the M-phase in wild-type clones (Fig. 3A′′, A′′′ and E), while PH3-positive mitotic Nbs were observed in 0/12 $Acsl^{KO}$ clones and 1/20 $Acsl^{1}$ clones (Fig. 3B′′, B′′′, C′′, C′′′ and E).

To determine if Nb loss occurs in MB clones specifically or more generally in clones of other types of Nbs, we quantified Nb number in type I Nb clones in the central brain. In wild type, all of the type I Nb clones contained a single Nb (Fig. S3A, A′ and D). But almost half of the Nb clones showed no Nb in $Acsl^{1}$ and $Acsl^{8}$ mutants (Figs. S3B–D). Consistently, the number of progeny cells was reduced significantly in *Acsl* mutant clones compared with wild type (Fig. S3E). These results together demonstrate that different types of Nbs are prematurely lost in *Acsl* mutants.

2.3. Acsl is required for Nb proliferation activity

Based on the MB Nb clonal analyses shown above, we suspected that the reduced Nb clone size was due to reduced proliferation activity of MB Nbs in *Acsl* mutants. To test this possibility, we performed 5-ethynyl-2′-deoxyuridine (EdU) incorporation assays to detect DNA synthesis at S-phase and quantified the number of EdU-positive MB Nbs per brain hemisphere at 0 h and 48 h APF. It is known that four MB Nbs in each brain hemisphere of wild-type *Drosophila* are present from embryonic stage until late pupal stage before being eliminated at about 96 h APF, while other Nbs stop proliferating at about 30 h APF (Truman and Bate, 1988; Ito and Hotta, 1992; Siegrist et al., 2010). However, the number of MB Nbs was significantly decreased by half in $Acsl^{8}/Acsl^{05847}$ mutants while the wild-type MB labeled by *OK107-Gal4*-driven mCD8-GFP contained four Nbs per brain hemisphere at 0 h APF (Fig. 4A–B′ and I). The number of MB Nbs in $Acsl^{8}/Acsl^{05847}$ mutants was also significantly fewer at 48 h APF compared with wild type (Fig. 4C–D′ and I); the reduction of MB Nb numbers in $Acsl^{8}/Acsl^{05847}$ mutants was exacerbated with development between 0 h and 48 h APF (Fig. 4I). At 0 h and 48 h APF, 100% and 92.6% of wild-type MB Nbs, respectively, were EdU-positive after 1 h of incorporation (Fig. 4J). In contrast, the percentages of EdU-positive MB Nbs were significantly reduced to 59.6% and 40.9% in $Acsl^{8}/Acsl^{05847}$ mutants at the two APF stages, respectively (Fig. 4J). Consistently, the number of Nbs and the percentage of EdU-positive Nbs in the central brain were both significantly decreased in $Acsl^{KO}/Acsl^{05847}$ mutants compared with wild type (Fig. S4).

To determine whether there was a mitotic defect in *Acsl* mutants, we quantified the number of mitotic MB Nbs in wild-type and *Acsl* mutant brains by staining for PH3. Wild-type brains exhibited percentages of 38.3% and 28.4% PH3-positive MB Nbs at 0 h APF and

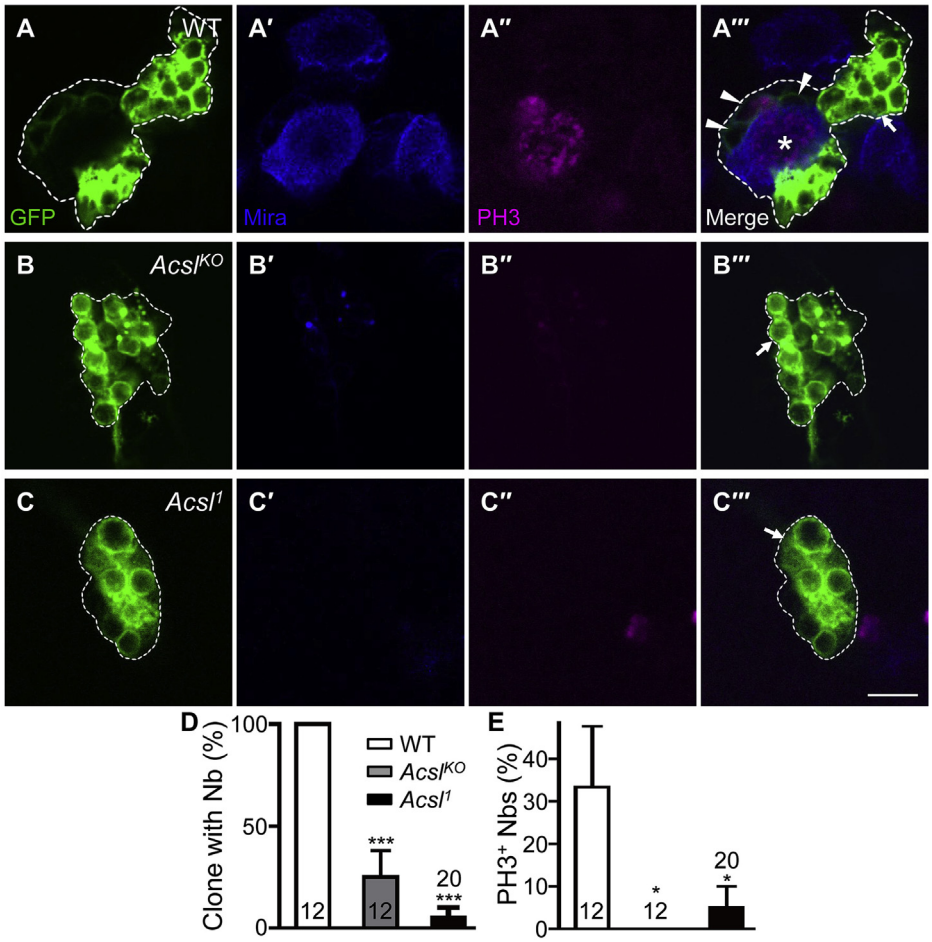

Fig. 3. Loss of Acsl results in Nb loss in the 3rd instar larval brain. **A**–**C‴**: MB Nb clones of wild type (**A**–**A‴**), $Acsl^{KO}$ (**B**–**B‴**) and $Acsl^{1}$ (**C**–**C‴**) mutants at the 3rd instar larval stage. Asterisk indicates MB Nbs, arrows indicate neurons, and arrowheads indicate GMCs which were weakly labled by mCD8-GFP. **D** and **E**: The percentage of clones with Nb (**D**) and the percentage of PH3-positive MB Nbs (**E**) were both significantly reduced in *Acsl* mutants. Error bars denote SEM; $^{*}P < 0.05$ and $^{***}P < 0.001$ by one-way ANOVA; the number of samples per genotype is listed in or above the bars. Scale bars, 10 μm.

48 h APF, respectively (Fig. 4E, E′, G, G′ and K), while $Acsl^{8}/Acsl^{05847}$ mutant brains showed percentages of 22.3% and 22.2% PH3-positive MB Nbs at 0 h APF and 48 h APF, respectively (Fig. 4F, F′, H, H′ and K). The percentage of PH3-positive MB Nbs showed a significant decrease in $Acsl^{8}/Acsl^{05847}$ mutants compared with wild type at 0 h APF, although it remained normal at 48 h APF (Fig. 4K). Taking these results together, we conclude that Acsl is required for Nb proliferation.

2.4. Loss of Acsl leads to reduced expression of Cyclin E in MB Nbs

As shown above, the percentages of EdU-positive Nbs were significantly decreased in *Acsl* mutants at pupal stages (Fig. 4). Cyclin E (CycE) plays a critical role in regulating the G1- to S-phase cell cycle transition (Lee and Orr-Weaver, 2003). Thus, we hypothesized that the decreased percentage of EdU-positive Nbs might be associated with reduced expression of CycE. To test this possibility, we performed immunostaining of CycE in MB Nbs at the 3rd instar larval stage. All 16 wild-type MB Nbs showed robust staining of CycE (average intensity in arbitrary units: 39.49; Fig. 5A–A″ and C). In contrast, eight $Acsl^{8}/Acsl^{05847}$ mutant MB Nbs showed significantly reduced staining of CycE (average intensity in arbitrary units: 8.54; Fig. 5B and C). These results support that the impaired proliferation activity in MB Nbs is associated with reduced CycE.

2.5. Loss of Acsl delays Nb cell cycle progression

To further define the cell cycle defect in *Acsl* mutants, we used time-lapse imaging to examine the MB Nb cell cycle within the intact larval brain (Lai et al., 2012; Cabernard and Doe, 2013). We imaged late 3rd instar larval MB Nbs in whole brain explants expressing mCD8-GFP by *OK107-Gal4* to monitor the nuclear and plasma membranes by confocal microscopy. Cell cycle times were determined between two consecutive events when a small new GMC was generated adjacent to the large parental Nb. In wild type, the cell cycle phases were determined based on cell shape and nuclear membrane morphology; for example, the start of interphase was characterized by plasma membrane fission and generation of a new GMC (Fig. 6A and B). The average MB Nb cell cycle time was about 38 min ($n = 8$; Fig. 6B; Movie 1), much faster than the cell cycle in both type I and type II Nbs of the central brain (Bowman et al., 2008; Cabernard and Doe, 2009; Poon et al., 2016). In contrast, $Acsl^{8}/Acsl^{05847}$ and $Acsl^{KO}/Acsl^{05847}$ mutant MB Nbs showed such a dramatically prolonged interphase that we did not observe a single complete cell cycle within the 7 h time window of

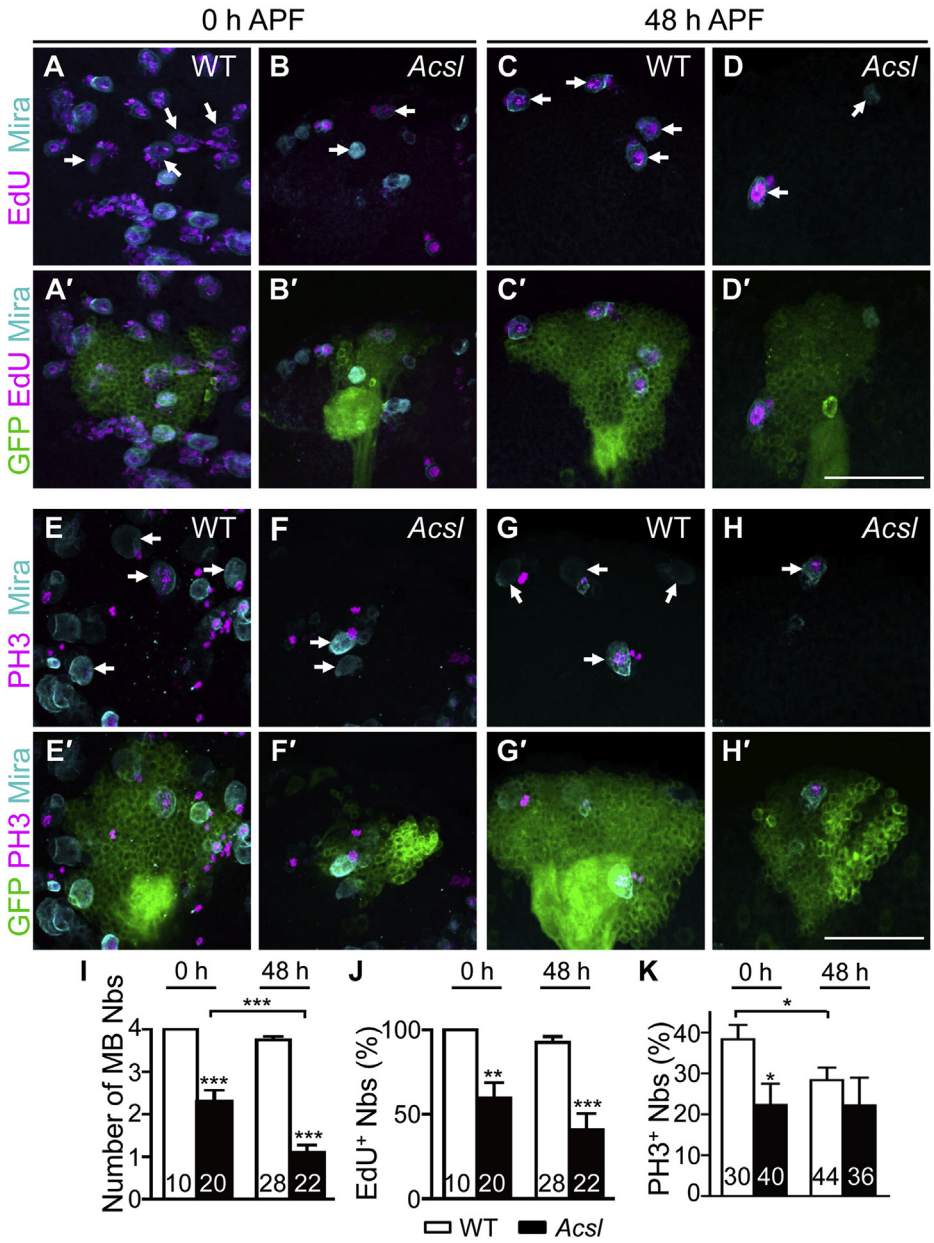

Fig. 4. Loss of Acsl leads to decreased proliferation activity of MB Nbs. **A**–**H**′: Projections of confocal images of pupal brains triple-labeled with anti-Mira (cyan), *OK107-Gal4>UAS-mCD8-GFP* (green), and EdU (magenta; **A**–**D**′) or anti-PH3 (magenta; **E**–**H**′). **A**, **C**, **E** and **G** are images from wild-type pupae while **B**, **D**, **F**, and **H** are images from $Acsl^{8}/Acsl^{05847}$ mutants. **I**: The number of MB Nbs in each brain hemisphere was significantly decreased in $Acsl^{8}/Acsl^{05847}$ mutants at both 0 h and 48 h APF compared with the wild type. **J**: The percentage of EdU-positive MB Nbs was significantly decreased in $Acsl^{8}/Acsl^{05847}$ mutants at both 0 h and 48 h APF compared with the wild type. **K**: The percentage of PH3-positive MB Nbs per brain was significantly decreased at 0 h but remained normal at 48 h APF in $Acsl^{8}/Acsl^{05847}$ mutants compared with the wild type. Error bars denote SEM; $^{*}P < 0.05$, $^{**}P < 0.01$ and $^{***}P < 0.001$ by Student's *t*-test; the number of samples per genotype is listed in the bars. Arrows indicate Nbs. Scale bars, 50 μm.

observation in at least 5 $Acsl^{8}/Acsl^{05847}$ and 5 $Acsl^{KO}/Acsl^{05847}$ larvae (Fig. 6C; Movie 2). We therefore were unable to determine the time for each complete cell cycle, as only one mitotic process was observed in 10 *Acsl* mutant brains examined. In addition, the diameters of MB Nbs in $Acsl^{8}/Acsl^{05847}$ and $Acsl^{KO}/Acsl^{05847}$ mutants were significantly smaller than wild type (13.64 ± 0.19 μm for wild type, 9.91 ± 0.48 μm for $Acsl^{8}/Acsl^{05847}$, $P < 0.001$ and 11.51 ± 0.91 μm for $Acsl^{KO}/Acsl^{05847}$, $P < 0.05$; Fig. 6D). Similar analysis revealed prolonged cell cycle in type I Nbs (160 ± 13 min for wild type, 313 ± 32 min for $Acsl^{KO}/Acsl^{05847}$, $P < 0.001$). Taken together, these data demonstrate that loss of Acsl results in a severe delay in Nb cell cycle progression.

Supplementary video related to this article can be found at https://doi.org/10.1016/j.jgg.2018.10.006.

2.6. Acsl prevents premature differentiation of Nbs by inhibiting nuclear localization of Pros

Nbs in the central brain stop proliferation via apoptosis or Prospero (Pros)-dependent cell-cycle exit during development (Bello et al., 2003; Cenci and Gould, 2005; Maurange et al., 2008; Siegrist et al., 2010). Apoptosis is unlikely the cause of MB Nb loss since neither blocking apoptosis by overexpressing p35, a potent inhibitor of caspases, nor removing the three pro-apoptotic genes

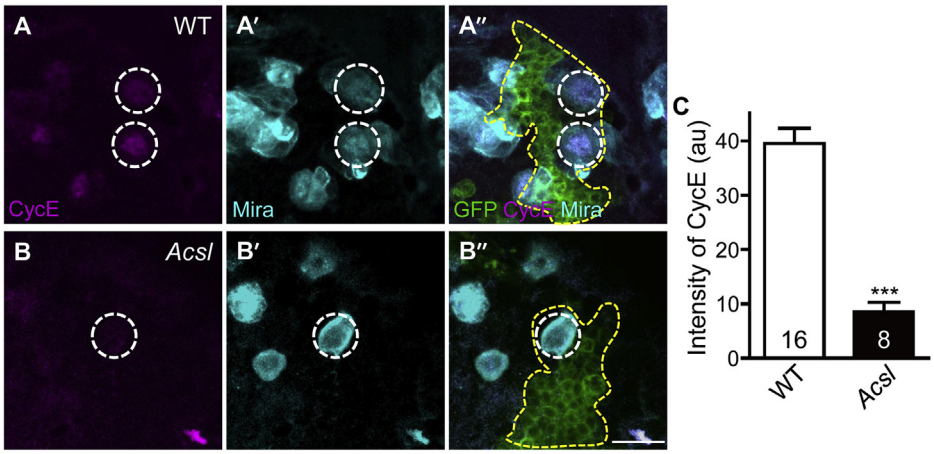

Fig. 5. Reduced CycE staining in *Acsl* mutant MB Nbs. **A**–**B**′′: MB Nbs at the 3rd instar larval stage of wild-type (WT) (**A**–**A**′′) and $Acsl^{8}/Acsl^{05847}$ mutants (**B**–**B**′′) were co-labeled by anti-Mira (cyan) and anti-CycE (magenta). MB was marked by mCD8-GFP driven by *OK107-Gal4*. **C**: The intensity of CycE staining was significantly reduced in $Acsl^{8}/Acsl^{05847}$ mutant Nbs. Error bars denote SEM; $^{***}P < 0.001$ by Student's *t*-tests; the number of samples per genotype is listed in the bars. Yellow dashed lines indicate MBs. Scale bars, 10 μm.

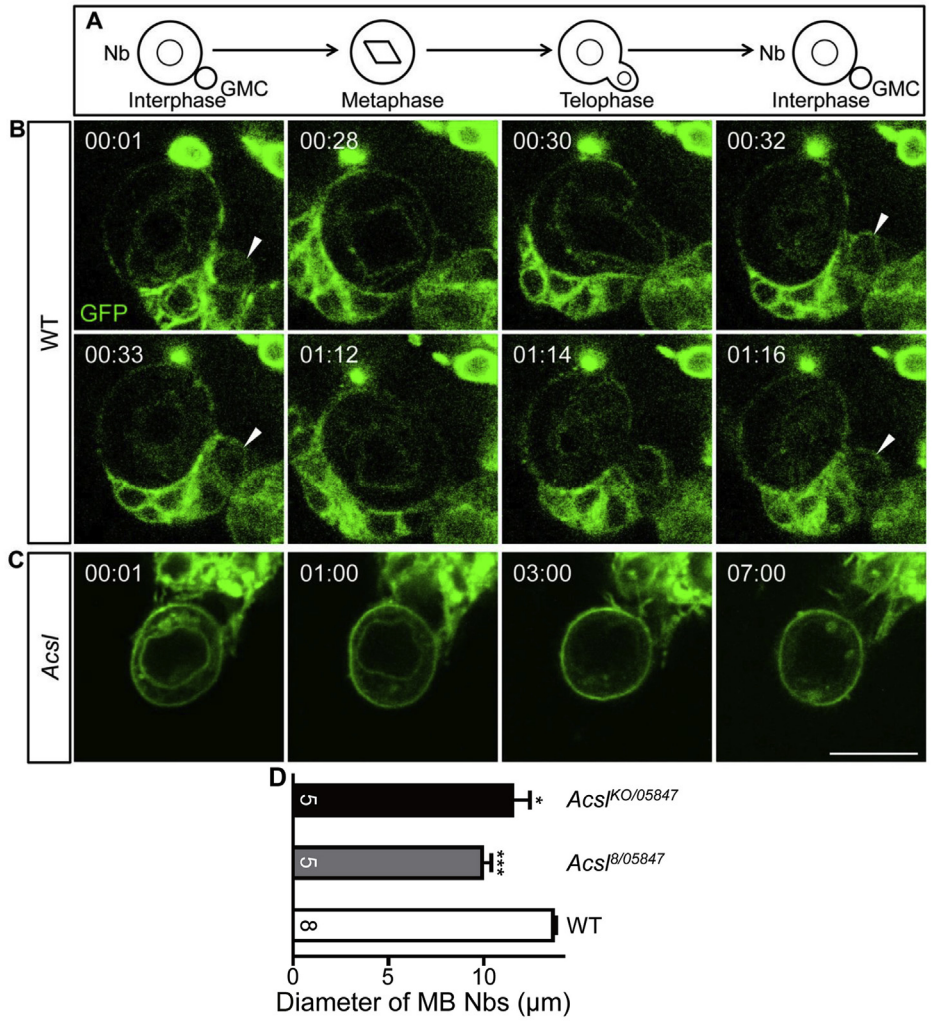

Fig. 6. Acsl is required for Nb cell cycle progression. **A**: Diagram of MB Nb cell cycle progression. The interphase, metaphase, and telophase of a complete Nb cell cycle can be clearly visualized by live imaging. MB Nbs were labeled with mCD8-GFP (green) driven by *OK107-Gal4*. **B** and **C**: Representative time-lapse images of MB Nb division in the brains of 3rd instar larvae of wild type (**B**) and $Acsl^{8}/Acsl^{05847}$ mutants (**C**). In the wild type (**B**), we observed the normal cell cycle completed in 32 min and 1 h 16 min. In contrast, in $Acsl^{8}/Acsl^{05847}$ mutants (**C**), the MB Nbs did not enter into mitosis within the 7 h time period we examined. Imaging time is indicated at the upper-left corner of each frame (h: min). $n = 8$ for wild type and $n = 5$ for $Acsl^{8}/Acsl^{05847}$ mutants. **D**: Quantification results of the average diameter of MB Nbs in the 3rd instar larval brain. Error bars denote SEM; $^{*}P < 0.05$ and $^{***}P < 0.001$ by one-way ANOVA; the number of samples per genotype is listed in the bars. Arrowheads indicate newly generated GMCs. Scale bars, 10 μm.

reaper, *hid* and *grim* by half by introducing heterozygous deficiency *Df(3L)H99* in $Acsl^{8}/Acsl^{05847}$ mutants rescued Nb loss (Fig. S6A–L and P). Furthermore, terminal deoxynucleotidyl transferase-mediated dUTP-biotin nick end labeling (TUNEL) assay did not detect apoptotic signal in *Acsl* mutant Nbs (Fig. S6M–O″).

Pros is a key molecule controlling the switch between a self-renewing and a differentiating Nb (Knoblich et al., 1995; Spana and Doe, 1995; Maurange et al., 2008). In the Nbs, the differentiation factor Pros is localized in the cytoplasm during interphase but enriched at the basal cortex during mitosis (Hirata et al., 1995; Knoblich et al., 1995; Spana and Doe, 1995). High levels of Pros in the nuclei trigger Nb differentiation (Choksi et al., 2006; Lai and Doe, 2014). To test if Pros is involved in the premature loss of Nbs in *Acsl* mutant brain, we examined whether Pros precociously accumulates in the nuclei of *Acsl* mutant Nbs. All 28 wild-type MB Nbs at 48 h APF showed no nuclear Pros (Fig. 7A–A″), whereas 10 of 36 (27.78%) MB Nbs showed nuclear Pros in $Acsl^{8}/Acsl^{05847}$ mutants (Fig. 7B–B″). We then sought to determine if the nuclear localization of Pros in *Acsl* mutant Nbs can be rescued by reducing the level of Pros. To this goal, we introduced a heterozygous $pros^{17}/+$ mutation which reduces Pros level by half in *Acsl* mutant background and found that the percentage of nuclear localization of Pros in $Acsl^{8}/Acsl^{05847}$ mutant MB Nbs was significantly rescued, though not to the wild-type level (Fig. 7C–C″ and G). Consistently, the number of Nbs in *Acsl* mutants was also significantly rescued by heterozygous $pros^{17}$ mutation (Fig. 7D–F′ and H). Taken together, our results show that premature differentiation rather than caspase-dependent cell apoptosis contributes to the loss of MB Nbs observed in *Acsl* mutants. We propose that Acsl maintains MB Nb stemness, at least partially, by inhibiting nuclear Pros localization.

2.7. Transcriptional profile is altered in Acsl mutant Nbs

Acsl converts long-chain fatty acids to acyl-CoAs and mutation of *Acsl* alters fatty acid and sphingolipid levels (Huang et al., 2016). Fatty acids, fatty acyl-CoAs or their metabolites can act as transcriptional ligands to regulate gene transcription (Grevengoed et al., 2014). Furthermore, Pros, a transcriptional factor, is mislocalizd in the nuclei of *Acsl* mutant Nbs (Fig. 7). To determine a potential role of *Acsl* in transcriptional regulation, we compared the transcriptional profile of wild-type and *Acsl* mutant Nbs. Fluorescence-activated cell sorting (FACS) was used to purify wild-type and *Acsl* mutant Nbs from late 3rd instar larval brains according to published protocols (Berger et al., 2012; Harzer et al., 2013) (Fig. S7A). Nbs were labeled by nls-GFP under the control of *insc-Gal4* which expresses in all Nbs. RNA from the FACS-sorted Nbs was sequenced to yield an average of 14.5 million clean reads per sample. Three independent biological replicates for each genotype were statistically analyzed. Comparison of the transcriptional profiles of wild-type and $Acsl^{KO}/Acsl^{05847}$ mutant Nbs using Cuffdiff algorithm identified 296 differentially expressed genes (false discovery rate (FDR) < 0.05; Table S1). Among these genes, 183 genes were upregulated and 113 genes were downregulated in *Acsl* mutant Nbs ($\log_2$ (fold change) > 1 or $\log_2$ (fold change) < −1) (Fig. S7C). To assess the

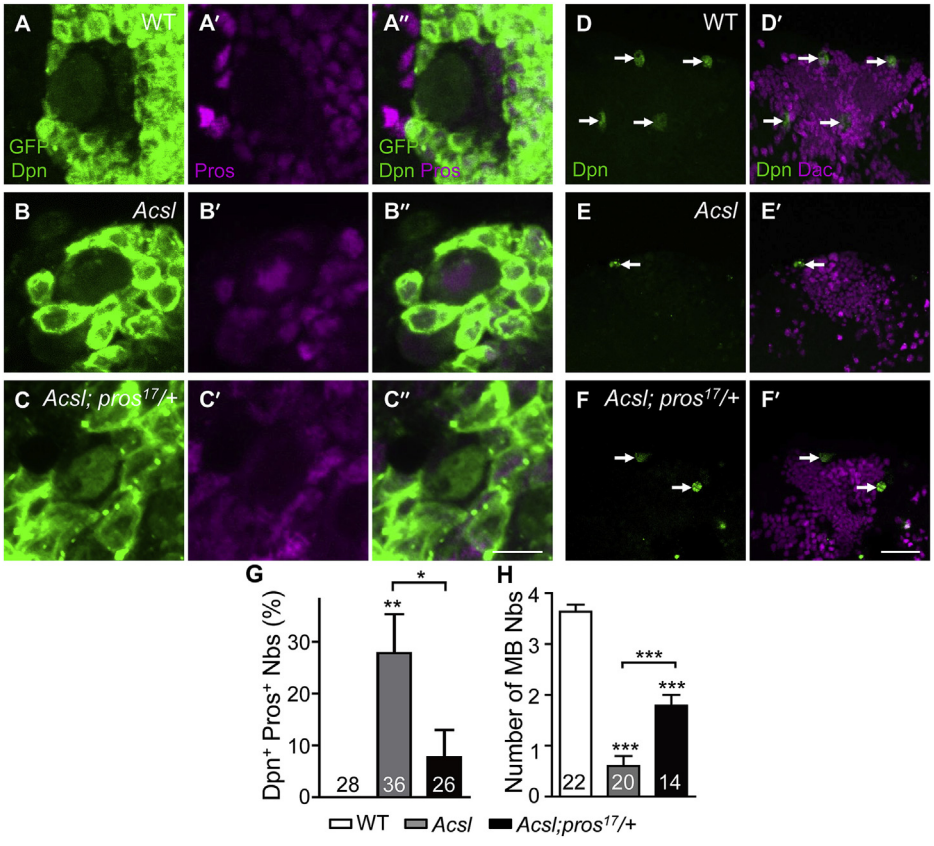

Fig. 7. Acsl prevents nuclear localization of Pros to maintain Nb stemness. **A**–**C**″: Pros was present in the MB Nb nucleus of $Acsl^{8}/Acsl^{05847}$ mutants (B–B″) but not in wild-type nuclei (**A**–**A**″) at 48 h APF. The *Acsl* mutant phenotypes were rescued by reducing Pros levels by half (**C**–**C**′). Nbs were labeled by anti-Dpn (green), while anti-Pros signals were displayed in magenta. The MB was marked by mCD8-GFP driven by *OK107-Gal4*. **D**–**F**′: Projected confocal images of 48 h APF MB co-labeled with anti-Dpn (green) and anti-Dac (magenta). **D** and **D**′: wild type. **E** and **E**′: $Acsl^{8}/Acsl^{05847}$. **F** and **F**′: $Acsl^{8}/Acsl^{05847}$; $pros^{17}/+$. **G**: The percentage of Dpn^{+} $Pros^{+}$ MB Nbs was significantly decreased in $Acsl^{8}/Acsl^{05847}$; $pros^{17}/+$ compared with $Acsl^{8}/Acsl^{05847}$ mutants at 48 h APF. **H**: Quantification results of the number of Nbs in each brain hemisphere at 48 h APF. Error bars denote SEM; $^{*}P < 0.05$, $^{**}P < 0.01$ and $^{***}P < 0.001$ by one-way ANOVA; the number of samples per genotype is listed in the bars. Scale bars, 10 μm (**A**–**C**″) and 20 μm (**D**–**F**′).

quality of the RNA-seq data, we verified the expression of selected genes by quantitative reverse transcription (qRT)-PCR. Consistent with RNA-seq results, qRT-PCR showed the same trend of transcriptional change for all 10 genes tested (Fig. S7D).

Gene ontology (GO) analysis revealed that the upregulated genes were enriched for neuronal differentiation and axonal guidance (Fig. 8A). Although we observed abnormal Pros localization in the nuclei of *Acsl* mutant Nbs, the level of *Pros* mRNA was not significantly increased, indicating *Acsl* does not regulate Pros at transcriptional level (Fig. 8B). Netrin-B, a secreted protein that requires Pros for proper expression and guides axon outgrowth (Mitchell et al., 1996; Choksi et al., 2006), was up-regulated ($\log_2$ (fold change) = 2.71, $q = 0.011$) in *Acsl* mutant Nbs. Cdk5α, which regulates neuronal projection and morphogenesis (Trunova et al., 2011), also showed increased mRNA level ($\log_2$ (fold change) = 2.18, $q = 0.004$) (Fig. 8B). GO analysis of the upregulated genes also revealed significant over-representation of genes in regulation of synapse organization (Fig. 8A).

On the other hand, the downregulated genes were over-represented in regulating the processes of mitotic cell cycle, chromosome segregation, protein folding and RNA processing (Fig. 8B). For example, *mei-38* ($\log_2$ (fold change) = −3.59, $q = 0.004$), *Klp67A* ($\log_2$ (fold change) = −1.84, $q = 0.004$), and *aurB* ($\log_2$ (fold change) = −1.55, $q = 0.021$) are involved in mitotic cell cycle and chromosome segregation (Giet and Glover, 2001; Gandhi et al., 2004; Wu et al., 2008; Roth et al., 2015), while *enok* ($\log_2$ (fold change) = −2.98, $q = 0.004$) and *partner of numb* (*pon*) ($\log_2$ (fold change) = −1.45, $q = 0.036$) are involved in Nb proliferation (Lu et al., 1998; Scott et al., 2001). The downregulated expression of cell cycle and Nb proliferation genes is consistent with the prolonged cell cycle and defective Nb activity in *Acsl* mutants.

In summary, RNA-seq results show downregulated cell fate and cell-cycle-related genes and upregulated differentiation genes in *Acsl* mutant Nbs, supporting that *Acsl* plays a critical role in regulating Nb proliferation and differentiation.

3. Discussion

3.1. Acsl is required for MB development in a cell autonomous manner

Mutations in *ACSL4* lead to non-syndromic ID, but how ACSL4 regulates brain development remains largely unexplored. In the present study, we show for the first time that *Drosophila* Acsl is required for MB development. A non-cell autonomous function has been reported for Acsl in the production of Dpp, one of the *Drosophila* BMP homologs in the larval brain (Zhang et al., 2009). Glial signals are necessary for Nb proliferation at late-larval stages

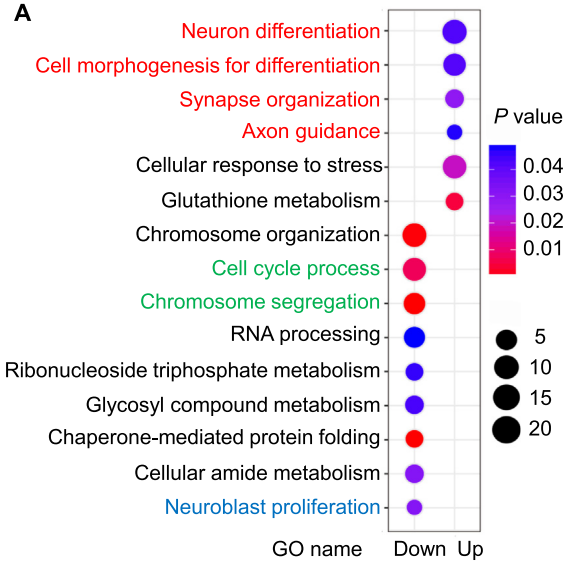

B

Gene	$\log_2$ (fold change)	*q* value
Neuroblast proliferation		
enok	-2.98	0.004
pon	-1.45	0.036
Cell cycle		
mei-38	-3.59	0.004
san	-2.38	0.004
corto	-2.09	0.015
CSN4	-1.88	0.004
Klp67A	-1.84	0.004
smt3	-1.79	0.024
RfC3	-1.74	0.043
Mis12	-1.68	0.036
borr	-1.64	0.021
mus101	-1.62	0.022
mus301	-1.55	0.048
aurB	-1.55	0.021
Neuronal differentiation		
rho	10.00	0.004
hairy	10.00	0.004
Rac2	10.00	0.004
Ten-m	3.13	0.033
nerfin-1	3.12	0.015
scrt	2.74	0.006
NetB	2.71	0.011
Spn	2.61	0.004
Lrrk	2.55	0.025
plum	2.49	0.004
RhoGAP100F	2.30	0.004
Cdk5α	2.18	0.004
futsch	2.15	0.015
Wnt4	2.03	0.043
pros	1.34	0.682*

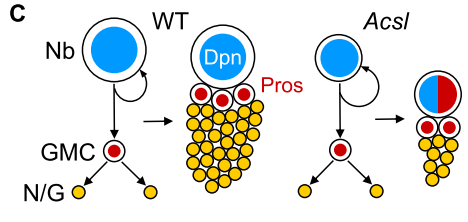

Fig. 8. Acsl regulates the Nb transcriptional profile. **A**: Scatterplot showing GO functional enrichment for differentially expressed genes. The color of the circles represents different *P* values (all *P* values < 0.05). The size of circles represents gene count. The raw RNA-seq sequencing data were deposited to Gene Expression Omnibus database with accession number GSE118275. **B**: List of the altered genes involved in Nb proliferation, cell cycle process and neuronal differentiation. *q* value denotes the minimum false discovery rate (FDR < 0.05) at which the change can be called significant. Asterisk indicates the change is not significant. See Table S1 for the full list. **C**: Diagram depicting the critical role of Acsl in Nb activity. In the wild type, a Nb divides asymmetrically to self-renew and generate a GMC which divides once to generate two neurons or glia. Nuclear Dpn is in light blue, while Pros is in red. In contrast to the wild type, *Acsl* mutant Nbs are smaller, take longer time to self-renew, and differentiates prematurely due to the presence of nuclear Pros, leading to fewer Nb progeny.

(Cheng et al., 2011). It is thus important to determine if Acsl regulates brain development in a cell autonomous or non-cell autonomous manner. Independent experiments show that *Acsl* is required for normal MB Nb activity in a cell autonomous manner. First, knockdown of *Acsl* in both Nbs and their neuronal progeny of MB by *OK107-Gal4*-driven RNAi recapitulated the mutant phenotypes. Conversely, *OK107-Gal4*-driven but not MB neuronal specific *30Y-Gal4*-driven expression of Acsl substantially rescued the mutant MB phenotypes. Second, MB Nb clonal analysis of multiple *Acsl* alleles showed a greatly reduced number of γ neurons and absence of later-born α′/β′ and α/β neurons. Together, these data demonstrate that Acsl is required for cell-autonomous MB development.

3.2. Acsl is required for Nb proliferation

It has been shown recently that lipogenesis plays an important role in regulating the activity of neural stem and progenitor cells (NSPCs, the mammalian equivalent of *Drosophila* Nbs) (Knobloch et al., 2013). Proliferating NSPCs show high level expression of fatty acid synthase (FASN), an enzyme that catalyses the production of palmitate which is a substrate for the synthesis of new fatty acids. On the contrary, slowly proliferating NSPCs show a high level expression of SPOT14, an inhibitor of malonyl-CoA synthesis and *de novo* lipogenesis. Consistently, neurogenesis in mouse NSPCs is impaired when FASN is conditionally deleted (Knobloch et al., 2013). Furthermore, fatty acids are metabolized in NSPCs of the subventricular zone to produce energy and support proliferation activity (Stoll et al., 2015). Thus, lipid biosynthesis plays a critical role in NSPC proliferation. In support of this conclusion, we show here that mutations in *Acsl*, which acts in a similar metabolic pathway as FASN, result in greatly reduced Nb proliferation activity. Our findings on Acsl, together with the mammalian studies, reveal the emerging importance of a lipid metabolic program in regulating neural stem cell activity.

How might Acsl regulate Nb proliferation activity? We found that MB Nb size was significantly reduced in *Acsl* mutants, which may explain impaired Nb proliferation. Reduced MB Nb size in *mushroom bodies tiny* (*mbt*) mutants is accompanied by reduced mitotic activity (Melzer et al., 2013), while an acceleration of the cell cycle is associated with increased cell size of Nbs when the Hippo pathway is disrupted (Poon et al., 2016). Thus, a reduction in cell size (Fig. 6), together with reduced expression of CycE (Fig. 5) and the cell proliferation genes *pon* and *enok* (Fig. 8), may contribute to the compromised proliferation of Nbs in *Acsl* mutants. RNA-seq results also showed downregulated cell cycle related genes such as *mei-38*, *Klp67A*, and *aurB* in *Acsl* mutant Nbs (Fig. 8), consistent with the prolonged cell cycle in *Acsl* mutants. Thus, multiple independent lines of evidence support Acsl is necessary for Nb proliferation activity.

3.3. Loss of Acsl leads to premature differentiation of MB Nbs

Normal brain development depends on tightly regulated initiation and termination of Nb proliferation. The proliferation of different types of Nbs is terminated by different means. MB Nbs survive much longer than Nbs in other parts of the brain. Before MB Nb elimination at approximately 96 h of pupal development, a decrease in insulin and PI3K signaling induces nuclear localization of the transcription factor FOXO, which reduces growth and proliferation of these Nbs (Siegrist et al., 2010). The resulting smaller Nbs are then eliminated by caspase-dependent cell death as determined by positive TUNEL staining, while prolonged survival of Nbs is observed after genetically inhibiting active caspases by p35 (Siegrist et al., 2010). Here we show that Acsl prevents premature differentiation of Nbs, a conclusion based in part on the upregulation of neuronal differentiation genes and downregulation of Nb and cell-cycle related genes, as well as nuclear localization of Pros in *Acsl* mutant Nbs. It has been reported that nuclear Pros represses self-renewal genes, such as stem cell fate genes and cell-cycle related genes, but activates terminal differentiation genes (Choksi et al., 2006). Specifically, Pros induces transcription of its direct targets including neuronal differentiation genes *NetB* and *rho*, both of which were found to be upregulated in *Acsl* mutants, though the mRNA level of *pros* was normal (Fig. 8B). Moreover, loss of one copy of *pros* partially but significantly rescued the decreased Nb numbers and the increased nuclear Pros localization in *Acsl* mutant Nbs. These results together support that Acsl prevents premature differentiation of Nbs through multiple molecular pathways including Pros. It remains to be clarified how Acsl inhibits Pros nuclear localization and premature differentiation of Nbs.

The MB Nbs don't undergo apoptosis in *Acsl* mutants, different from reports of other mutants. For example, mutants of *worniu* (*wor*), which encodes a zinc finger transcription factor of the Slug/Snail family, show prolonged cell cycle with a striking delay in mitosis (Lai et al., 2012). Loss of Nbs seen in *wor* mutants is largely due to apoptosis (Lai et al., 2012). *wor* mutant Nbs also differentiate prematurely evidenced by an abnormally high level of expression of the neuronal differentiation marker Elav in Nb nuclei (Lai et al., 2012). Mutants of *mushroom bodies tiny* (*mbt*), which encodes the p21-activated kinase, also show premature loss of MB Nbs due to apoptosis (Melzer et al., 2013). In *dpn* mutants, however, Nbs loss is caused by premature differentiation due to nuclear accumulation of Pros, rather than apoptosis (Zhu et al., 2012), similar to what we observed in *Acsl* mutants. It would be interesting to uncover the molecular underpinnings that are involved in the closely similar Nb phenotypes of *Acsl* and *dpn* mutants.

In summary, our findings unravel a critical and previously unknown role of Acsl in regulating Nb activity. The next challenge will be to identify and define the molecules or molecular pathways that mediate the essential function of Acsl in Nbs.

4. Materials and methods

4.1. Fly stocks and husbandry

Flies were cultured on standard cornmeal medium at 25 °C. w^{1118} was used as wild-type control if not specified otherwise. The *Acsl* null allele $Acsl^{KO}$, three *Acsl* hypomorphic alleles $Acsl^{05847}$, $Acsl^{8}$, and $Acsl^{1}$, a UAS line expressing *Drosophila* Acsl, two UAS lines each expressing wild-type or mutant human ACSL4, and an *Acsl-RNAi* line were described previously (Zhang et al., 2009; Liu et al., 2011, 2014). Neural *elav-Gal4*, Nb specific *insc-Gal4*, MB specific *OK107-Gal4*, *30Y-Gal4*, *c305a-Gal4*, *mb247-Gal4*, *UAS-mCD8-GFP*, *UAS-CycE*, *UAS-nls-GFP*, *UAS-p35*, *UAS-nls-GFP*, *Df(3L)H99* and $pros^{17}$ were obtained from Bloomington Stock Center, USA. Core α/β subdivision specific *NP7175-Gal4* was obtained from Kyoto Stock Center, Japan.

For MARCM analysis, we followed established protocols (Lee et al., 1999; Lee and Luo, 1999). *FRTG13* and *hsFLP elav-Gal4; FRTG13 tubP-Gal80* were obtained from the Bloomington Stock Center. The following *Drosophila* strains were generated by standard genetic methods: 1) *FRTG13* $Acsl^{KO}$/*CyO-GFP*, 2) *FRTG13* $Acsl^{8}$/*CyO-GFP*, 3) *FRTG13* $Acsl^{1}$/*CyO-GFP*, 4) *FRTG13; UAS-Acsl-Myc/TM6B*, 5) *FRTG13; UAS-ACSL4-Myc/TM6B*, 6) *FRTG13* $Acsl^{KO}$/*CyO-GFP; UAS-Acsl-Myc/TM6B*, 7) *FRTG13* $Acsl^{KO}$/*CyO-GFP; UAS-ACSL4-Myc/TM6B*, and 8) *hsFLP UAS-mCD8-GFP elav-Gal4; FRTG13 tubP-Gal80/CyO-GFP*.

4.2. MARCM analysis

For MARCM analysis, embryos were collected within a 2 h time

window and cultured at 25 °C. The following *Drosophila* strains were heat shocked at 37 °C for 3 h after larval hatching (ALH) and examined at 3rd instar larva or adult stages. The genotypes for clonal analysis were: 1) *hsFLP UAS-mCD8-GFP elav-Gal4/+; FRTG13 tubP-Gal80/FRTG13*, 2) *hsFLP UAS-mCD8-GFP elav-Gal4/+; FRTG13 tubP-Gal80/FRTG13 Acsl^{KO}*, 3) *hsFLP UAS-mCD8-GFP elav-Gal4/+; FRTG13 tubP-Gal80/FRTG13 Acsl^{8}*, 4) *hsFLP UAS-mCD8-GFP elav-Gal4/+; FRTG13 tubP-Gal80/FRTG13 Acsl^{1}*, 5) *hsFLP UAS-mCD8-GFP elav-Gal4/+; FRTG13 tubP-Gal80/FRTG13 Acsl^{KO}; UAS-Acsl-Myc/+*, and 6) *hsFLP UAS-mCD8-GFP elav-Gal4/+; FRTG13 tubP-Gal80/FRTG13 Acsl^{KO}; UAS-ACSL4-Myc/+*.

To generate type I Nb clones, the following *Drosophila* strains were heat shocked at 37 °C during 12–18 h after larval hatching (ALH) and examined at 3rd instar larva stage. The genotypes for MARCM clonal analysis were 1) *hsFLP UAS-mCD8-GFP elav-Gal4/+; FRTG13 tubP-Gal80/FRTG13*, 2) *hsFLP UAS-mCD8-GFP elav-Gal4/+; FRTG13 tubP-Gal80/FRTG13 Acsl^{8}*, 3) *hsFLP UAS-mCD8-GFP elav-Gal4/+; FRTG13 tubP-Gal80/FRTG13 Acsl^{1}*.

For quantification of neuron number in MARCM clones, serial confocal images without overexposure through the whole clone were analyzed as previously described (Lee et al., 1999).

4.3. Immunohistochemistry analysis and confocal microscopy

Brains at specific developmental stages were dissected in cold PBS and fixed in 4% paraformaldehyde on ice for 30 min. For anti-Dpn staining, brains were fixed with 4% paraformaldehyde in PEM buffer (100 mM Pipes (pH 6.9), 1 mM EGTA, 1 mM $MgCl_2$) containing 0.3% Triton X-100 (PBST) for 25 min. After washed by PBS with 0.5% Triton X-100 (PBST), brains were blocked in 0.5% PBST with 5% normal goat serum (NGS) at room temperature and incubated with primary antibodies diluted in 0.5% PBST containing 5% NGS overnight at 4 °C, followed by incubating with secondary antibodies for 3 h at room temperature. The following primary antibodies were used: mouse anti-FasII (1:20; Developmental Studies Hybridoma Bank (DSHB), USA), rat anti-mCD8 (1:100; Life Technologies, USA), rabbit anti-PH3 (1:1000; Millipore, USA), rabbit anti-Mira (1:2000; F. Matsuzaki, Kobe, Japan), mouse anti-Mira (1:20; F. Matsuzaki), guinea pig anti-Dpn (1:500; James B. Skeath, Missouri, USA), rat anti-Dpn (1:100; Abcam, USA), rat anti-CycE (1:100; H. Richardson, Melbourne, Australia), mouse anti-Pros (1:1000; DSHB), and mouse anti-Dac (1:40; DSHB). Secondary antibodies used in this study were conjugated by Alexa Fluor 488, Cy3 or Alexa Fluor 633 (Molecular Probes, USA). All images were collected using an Olympus FV1000 laser scanning confocal microscope and processed with Adobe Photoshop CS4.

For statistical analysis of CycE staining intensity, *Acsl* mutant larval brains were processed in the same reaction tube as wild type. The CycE intensity of immunostaining in Nbs was quantified from projections of a series of sections through the entire MB Nbs by ImageJ. The fluorescence intensity was presented as arbitrary units (au).

For TUNEL analysis, brains were dissected in cold PBS and immediately fixed with 4% paraformaldyhyde for 30 min at room temperature. After washed by PBS with 0.2% Triton X-100 (PBS-T), brains were permeabilized by incubation in 1 × PBS containing 0.1% sodium citrate and 0.1% Triton X-100 on ice for 2 min and washed 3 times in 1 × PBST (0.2% Triton X-100) for 30 min. The nick-end labeling reaction was performed as recommended by the supplier (Roche, Switzerland) at 37 °C for 1 h.

4.4. EdU incorporation assay

EdU incorporation experiments were adapted from described previously (Poon et al., 2016). The Click-iT EdU Alexa Fluor 555 and 647 Imaging Kit (C10338, C10640, Life Technologies) were used. Dissected brains at different developmental stages were incubated in Schneider's *Drosophila* medium (21720024, Gibco, USA) complemented with EdU at a final concentration of 10 μM. Brains were then fixed and immunostained as described above. EdU was detected following manufacturer's instructions.

4.5. Time-lapse analysis of cell cycle progression of larval MB Nbs

Brains of wild-type and *Acsl* mutants at 3rd instar larval stage expressing mCD8-GFP by the MB specific *OK107-Gal4* were dissected and transferred to the tissue culture dish. Brains were then mounted in Schneider's *Drosophila* medium supplemented with 10% fetal bovine serum (10099141, Gibco) and Penicillin-Streptomycin (15070063, Gibco), and covered with a gas-permeable membrane (5793, YSI Life Sciences, USA). MB Nbs were imaged using an Olympus FV1000 laser scanning confocal microscope equipped with a 100 × 1.40 NA oil-immersion objective. Images were acquired every 1.5–3 min for 8 h with a spacing of 1 μm between Z-sections. Time-lapse images were processed using ImageJ and converted into movies.

4.6. Purification of Nbs by fluorescence-activated cell sorting (FACS)

FACS was carried out according to published protocols with minor modifications (Berger et al., 2012; Harzer et al., 2013). Briefly, we used *insc-gal4>nls-GFP* (nuclear located GFP) to label Nbs. Third instar larva were washed first in 70% ethanol and then in PBS. Intact brains without attached discs were dissected in cold supplemented Schneider's medium (10% fetal bovine serum, 2% Pen/Strep, 0.02 mg/mL insulin, 20 mM glutamine, 0.04 mg/mL glutathione, Schneider's *Drosophila* medium). Approximately fifty larval brains were washed twice in cold Rinaldini solution (Ceron et al., 2006) and incubated in supplemented Schneider's medium with the addition of 1 mg/mL collagenase I and 1 mg/mL papain (C0130 and P4762, respectively; Sigma Aldrich, USA) for 1 h at 30 °C. After washed with Rinaldini solution and supplemented Schneider's medium, brains were disrupted manually with a pipette tip in 200 μL supplemented Schneider's medium. The disrupted cell suspension was forced through a cell-strainer FACS tube and then subjected to FACS sorting. Nbs were sorted with a FACS AriaII machine (BD, USA) with a 100 mm nozzle and low pressure (20 psi) according to cell size and GFP intensity. For RNA isolation, 3000 Nbs sorted from wild-type and *Acsl* brains were collected in a 2.0 mL tube filled with 350 μL lysis buffer (74004, Qiagen, Germany).

4.7. RNA/cDNA preparation, RNA-seq and data analysis

Total RNA of ~3 ng from Nbs was isolated using RNeasy Micro Kit (74004, Qiagen) following the manufacturer's instructions. The quality of extracted RNA was examined on an Agilent 2100 Bio-Analyzer using the RNA 6000 Pico Kit (5067-1513, Agilent, USA). Since the 28S rRNA of insects breaks into two similar-sized fragments after heat-denaturation, which migrated closely to 18S rRNA, RNA electrophoretic profile with two sharp peaks and little or no baseline signals suggests high RNA integrity. RNA samples with high integrity were immediately converted to cDNA using REPLI-g® WTA Single Cell kit (150063, Qiagen). Poly A mRNAs were PCR-amplified by Oligo-dT primers. Transcriptome sequencing of the generated cDNA libraries using the 150-bp paired-end Illumina HiSeq 2500 system (Novogene Bioinformatics Technology Co., Ltd, China) yielded an average of 14.5 million clean reads per sample. All rRNA reads were removed by alignment against known rRNA sequences (RefSeq) and the remaining paired-end reads were aligned against the UCSC *D. melanogaster* genome (dm3) using Hisat (Kim

et al., 2015; Pertea et al., 2016). The number of fragments per kilobase of combined exon length per one million of total mapped reads (FPKM value) was used to estimate gene expression level. Transcriptional profile comparison between wild type and *Acsl* mutants was performed using Cuffdiff algorithm (Trapnell et al., 2012). Functional enrichment analysis of the differentially expressed genes was performed via DAVID web tool (Huang et al., 2009). We applied the 'functional annotation' function considering only 'biological process' (BP) ontologies. BP Ontologies were visualized using the R package (Ihaka and Gentleman, 1996).

4.8. Experimental design and statistical analysis

The gender of flies used in this study was random. Confocal images were analyzed by ImageJ Software. All statistical comparisons were performed using GraphPad InStat 5 software. One-way ANOVA was used to compare multiple group means. Student's *t*-tests were used for statistical comparisons between two groups. For statistical analysis, mean and standard error of the mean (SEM) values were calculated by standard methods. $P < 0.05$ was considered as a significant change. Asterisks above a column in figures show comparisons between a specific genotype and wild type, whereas asterisks above a bracket in figures denote comparisons between two specific genotypes.

Acknowledgments

We are grateful to F. Matsuzaki, James B. Skeath, H. Richardson, the Developmental Studies Hybridoma Bank at the University of Iowa, the Tsinghua University RNAi Center, the Kyoto Stock Center and the Bloomington Stock Center for antibodies and fly stocks. We thank Yan Song, Zhaohui Wang, and Zhiheng Xu for thoughtful discussion and comments. This work was supported by the grants from the Ministry of Science and Technology (2016YFA0501000), the National Science Foundation of China to YQZ (31490592) and AY (31271121).

Supplementary data

Supplementary data to this article can be found online at https://doi.org/10.1016/j.jgg.2018.10.006.

References

An, H., Ge, W., Xi, Y., Yang, X., 2017. Inscuteable maintains type I neuroblast lineage identity via Numb/Notch signaling in the *Drosophila* larval brain. J. Genet. Genomics 44, 151–162.

Bello, B.C., Hirth, F., Gould, A.P., 2003. A pulse of the *Drosophila* Hox protein abdominal-A schedules the end of neural proliferation via neuroblast apoptosis. Neuron 37, 209–219.

Berger, C., Harzer, H., Burkard, T.R., Steinmann, J., van der Horst, S., Laurenson, A.S., Novatchkova, M., Reichert, H., Knoblich, J.A., 2012. FACS purification and transcriptome analysis of *Drosophila* neural stem cells reveals a role for Klumpfuss in self-renewal. Cell Rep. 2, 407–418.

Bowman, S.K., Rolland, V., Betschinger, J., Kinsey, K.A., Emery, G., Knoblich, J.A., 2008. The tumor suppressors brat and numb regulate transit-amplifying neuroblast lineages in *Drosophila*. Dev. Cell 14, 535–546.

Cabernard, C., Doe, C.Q., 2009. Apical/Basal spindle orientation is required for neuroblast homeostasis and neuronal differentiation in *Drosophila*. Dev. Cell 17, 134–141.

Cabernard, C., Doe, C.Q., 2013. Live imaging of neuroblast lineages within intact larval brains in *Drosophila*. Cold Spring Harb. Protoc. 2013, 970–977.

Cao, Y., Murphy, K.J., McIntyre, T.M., Zimmerman, G.A., Prescott, S.M., 2000. Expression of fatty acid-CoA ligase 4 during development and in brain. FEBS Lett. 467, 263–267.

Cenci, C., Gould, A.P., 2005. *Drosophila* Grainyhead specifies late programmes of neural proliferation by regulating the mitotic activity and Hox-dependent apoptosis of neuroblasts. Development 132, 3835–3845.

Ceron, J., Tejedor, F.J., Moya, F., 2006. A primary cell culture of *Drosophila* post-embryonic larval neuroblasts to study cell cycle and asymmetric division. Eur. J. Cell Biol. 85, 567–575.

Cheng, L.Y., Bailey, A.P., Leevers, S.J., Ragan, T.J., Driscoll, P.C., Gould, A.P., 2011. Anaplastic lymphoma kinase spares organ growth during nutrient restriction in *Drosophila*. Cell 146, 435–447.

Choksi, S.P., Southall, T.D., Bossing, T., Edoff, K., de Wit, E., Fischer, B.E., van Steensel, B., Micklem, G., Brand, A.H., 2006. Prospero acts as a binary switch between self-renewal and differentiation in *Drosophila* neural stem cells. Dev. Cell 11, 775–789.

Crittenden, J.R., Skoulakis, E.M.C., Han, K.-A., Kalderon, D., Davis, R.L., 1998. Tripartite mushroom body architecture revealed by antigenic markers. Learn. Mem. 5, 38–51.

Gandhi, R., Bonaccorsi, S., Wentworth, D., Doxsey, S., Gatti, M., Pereira, A., 2004. The *Drosophila* kinesin-like protein KLP67A is essential for mitotic and male meiotic spindle assembly. Mol. Biol. Cell 15, 121–131.

Giet, R., Glover, D.M., 2001. *Drosophila* aurora B kinase is required for histone H3 phosphorylation and condensin recruitment during chromosome condensation and to organize the central spindle during cytokinesis. J. Cell Biol. 152, 669–682.

Grevengoed, T.J., Klett, E.L., Coleman, R.A., 2014. Acyl-CoA metabolism and partitioning. Annu. Rev. Nutr. 34, 1–30.

Harzer, H., Berger, C., Conder, R., Schmauss, G., Knoblich, J.A., 2013. FACS purification of *Drosophila* larval neuroblasts for next-generation sequencing. Nat. Protoc. 8, 1088–1099.

Heisenberg, M., 2003. Mushroom body memoir: from maps to models. Nat. Rev. Neurosci. 4, 266–275.

Hirata, J., Nakagoshi, H., Nabeshima, Y., Matsuzaki, F., 1995. Asymmetric segregation of the homeodomain protein Prospero during *Drosophila* development. Nature 377, 627–630.

Homem, C.C.F., Knoblich, J.A., 2012. *Drosophila* neuroblasts: a model for stem cell biology. Development 139, 4297–4310.

Homem, C.C.F., Repic, M., Knoblich, J.A., 2015. Proliferation control in neural stem and progenitor cells. Nat. Rev. Neurosci. 16, 647–659.

Huang, D.W., Sherman, B.T., Lempicki, R.A., 2009. Systematic and integrative analysis of large gene lists using DAVID bioinformatics resources. Nat. Protoc. 4, 44–57.

Huang, Y., Huang, S., Lam, S.M., Liu, Z., Shui, G., Zhang, Y.Q., 2016. Acsl, the *Drosophila* ortholog of intellectual-disability-related ACSL4, inhibits synaptic growth by altered lipids. J. Cell Sci. 129, 4034–4045.

Ihaka, R., Gentleman, R., 1996. R: a language for data analysis and graphics. J. Comput. Graph Stat. 5, 299–314.

Ikeshima-Kataoka, H., Skeath, J.B., Nabeshima, Y., Doe, C.Q., Matsuzaki, F., 1997. Miranda directs Prospero to a daughter cell during *Drosophila* asymmetric divisions. Nature 390, 625–629.

Ito, K., Hotta, Y., 1992. Proliferation pattern of postembryonic neuroblasts in the brain of *Drosophila melanogaster*. Dev. Biol. 149, 134–148.

Ito, K., Awano, W., Suzuki, K., Hiromi, Y., Yamamoto, D., 1997. The *Drosophila* mushroom body is a quadruple structure of clonal units each of which contains a virtually identical set of neurones and glial cells. Development 124, 761–771.

Kim, D., Langmead, B., Salzberg, S.L., 2015. HISAT: a fast spliced aligner with low memory requirements. Nat. Methods 12, 357–360.

Knoblich, J.A., Jan, L.Y., Jan, Y.N., 1995. Asymmetric segregation of numb and Prospero during cell-division. Nature 377, 624–627.

Knobloch, M., Braun, S.M.G., Zurkirchen, L., von Schoultz, C., Zamboni, N., Arauzo-Bravo, M.J., Kovacs, W.J., Karalay, O., Suter, U., Machado, R.A.C., Roccio, M., Lutolf, M.P., Semenkovich, C.F., Jessberger, S., 2013. Metabolic control of adult neural stem cell activity by Fasn-dependent lipogenesis. Nature 493, 226–230.

Kunz, T., Kraft, K.F., Technau, G.M., Urbach, R., 2012. Origin of *Drosophila* mushroom body neuroblasts and generation of divergent embryonic lineages. Development 139, 2510–2522.

Lai, S.L., Doe, C.Q., 2014. Transient nuclear Prospero induces neural progenitor quiescence. eLife 3, e03363.

Lai, S.L., Miller, M.R., Robinson, K.J., Doe, C.Q., 2012. The Snail family member Worniu Is continuously required in neuroblasts to prevent Elav-induced premature differentiation. Dev. Cell 23, 849–857.

Lee, L.A., Orr-Weaver, T.L., 2003. Regulation of cell cycles in *Drosophila* development: intrinsic and extrinsic cues. Annu. Rev. Genet. 37, 545–578.

Lee, T., Luo, L.Q., 1999. Mosaic analysis with a repressible cell marker for studies of gene function in neuronal morphogenesis. Neuron 22, 451–461.

Lee, T., Lee, A., Luo, L.Q., 1999. Development of the *Drosophila* mushroom bodies: sequential generation of three distinct types of neurons from a neuroblast. Development 126, 4065–4076.

Liu, Z.H., Huang, Y., Zhang, Y., Chen, D., Zhang, Y.Q., 2011. *Drosophila* Acyl-CoA synthetase long-chain family member 4 regulates axonal transport of synaptic vesicles and is required for synaptic development and transmission. J. Neurosci. 31, 2052–2063.

Liu, Z.H., Huang, Y., Hu, W., Huang, S., Wang, Q.F., Han, J.H., Zhang, Y.Q., 2014. dAcsl, the *Drosophila* ortholog of Acyl-CoA synthetase long-chain family member 3 and 4, inhibits synapse growth by attenuating bone morphogenetic protein signaling via endocytic recycling. J. Neurosci. 34, 2785–2796.

Longo, I., Frints, S.G.M., Fryns, J.P., Meloni, I., Pescucci, C., Ariani, F., Borghgraef, M., Raynaud, M., Marynen, P., Schwartz, C., Renieri, A., Froyen, G., 2003. A third MRX family (MRX68) is the result of mutation in the long chain fatty acid-CoA ligase 4 (*FACL4*) gene: proposal of a rapid enzymatic assay for screening mentally retarded patients. J. Med. Genet. 40, 11–17.

Lu, B., Rothenberg, M., Jan, L.Y., Jan, Y.N., 1998. Partner of Numb colocalizes with Numb during mitosis and directs Numb asymmetric localization in *Drosophila*

neural and muscle progenitors. Cell 95, 225–235.
Maurange, C., Cheng, L., Gould, A.P., 2008. Temporal transcription factors and their targets schedule the end of neural proliferation in *Drosophila*. Cell 133, 891–902.
Meloni, I., Parri, V., De Filippis, R., Ariani, F., Artuso, R., Bruttini, M., Katzaki, E., Longo, I., Mari, F., Bellan, C., Dotti, C.G., Renieri, A., 2009. The Xlmr gene *Acsl4* plays a role in dendritic spine architecture. Neuroscience 159, 657–669.
Meloni, I., Muscettola, M., Raynaud, M., Longo, I., Bruttini, M., Moizard, M.P., Gomot, M., Chelly, J., des Portes, V., Fryns, J.P., Ropers, H.H., Magi, B., Bellan, C., Volpi, N., Yntema, H.G., Lewis, S.E., Schaffer, J.E., Renieri, A., 2002. FACL4, encoding fatty acid-CoA ligase 4, is mutated in nonspecific X-linked mental retardation. Nat. Genet. 30, 436–440.
Melzer, J., Kraft, K.F., Urbach, R., Raabe, T., 2013. The p21-activated kinase Mbt is a component of the apical protein complex in central brain neuroblasts and controls cell proliferation. Development 140, 1871–1881.
Ming, G.-l., Song, H., 2011. Adult neurogenesis in the mammalian brain: significant answers and significant questions. Neuron 70, 687–702.
Mitchell, K.J., Doyle, J.L., Serafini, T., Kennedy, T.E., Tessier-Lavigne, M., Goodman, C.S., Dickson, B.J., 1996. Genetic analysis of Netrin genes in *Drosophila*: netrins guide CNS commissural axons and peripheral motor axons. Neuron 17, 203–215.
Pertea, M., Kim, D., Pertea, G.M., Leek, J.T., Salzberg, S.L., 2016. Transcript-level expression analysis of RNA-seq experiments with HISAT, StringTie and Ballgown. Nat. Protoc. 11, 1650–1667.
Poon, C.L., Mitchell, K.A., Kondo, S., Cheng, L.Y., Harvey, K.F., 2016. The Hippo pathway regulates neuroblasts and brain size in *Drosophila melanogaster*. Curr. Biol. 26, 1034–1042.
Ropers, H.H., 2008. Genetics of intellectual disability. Curr. Opin. Genet. Dev. 18, 241–250.
Ropers, H.H., Hamel, B.C.J., 2005. X-linked mental retardation. Nat. Rev. Genet. 6, 46–57.
Roth, M., Roubinet, C., Ifflander, N., Ferrand, A., Cabernard, C., 2015. Asymmetrically dividing *Drosophila* neuroblasts utilize two spatially and temporally independent cytokinesis pathways. Nat. Commun. 6, 6551.
Scott, E.K., Lee, T., Luo, L.Q., 2001. *Enok* encodes a *Drosophila* putative histone acetyltransferase required for mushroom body neuroblast proliferation. Curr. Biol. 11, 99–104.
Shen, C.P., Jan, L.Y., Jan, Y.N., 1997. Miranda is required for the asymmetric localization of Prospero during mitosis in *Drosophila*. Cell 90, 449–458.
Siegrist, S.E., Hague, N.S., Chen, C.H., Hay, B.A., Hariharan, I.K., 2010. Inactivation of both foxo and reaper promotes long-term adult neurogenesis in *Drosophila*. Curr. Biol. 20, 643–648.
Sousa-Nunes, R., Cheng, L.Y., Gould, A.P., 2010. Regulating neural proliferation in the *Drosophila* CNS. Curr. Opin. Neurobiol. 20, 50–57.
Spana, E.P., Doe, C.Q., 1995. The Prospero transcription factor is asymmetrically localized to the cell cortex during neuroblast mitosis in *Drosophila*. Development 121, 3187–3195.
Stoll, E.A., Makin, R., Sweet, I.R., Trevelyan, A.J., Miwa, S., Horner, P.J., Turnbull, D.M., 2015. Neural stem cells in the adult subventricular zone oxidize fatty acids to produce energy and support neurogenic activity. Stem Cell 33, 2306–2319.
Tastan, O.Y., Liu, J.L., 2015. CTP synthase is required for optic lobe homeostasis in *Drosophila*. J. Genet. Genomics 42, 261–274.
Trapnell, C., Roberts, A., Goff, L., Pertea, G., Kim, D., Kelley, D.R., Pimentel, H., Salzberg, S.L., Rinn, J.L., Pachter, L., 2012. Differential gene and transcript expression analysis of RNA-seq experiments with TopHat and Cufflinks. Nat. Protoc. 7, 562–578.
Truman, J.W., Bate, M., 1988. Spatial and temporal patterns of neurogenesis in the central nervous-system of *Drosophila melanogaster*. Dev. Biol. 125, 145–157.
Trunova, S., Baek, B., Giniger, E., 2011. Cdk5 regulates the size of an axon initial segment-like compartment in mushroom body neurons of the *Drosophila* central brain. J. Neurosci. 31, 10451–10462.
Vissers, L.E.L.M., Gilissen, C., Veltman, J.A., 2016. Genetic studies in intellectual disability and related disorders. Nat. Rev. Genet. 17, 9–18.
Wu, C., Singaram, V., McKim, K.S., 2008. mei-38 is required for chromosome segregation during meiosis in *Drosophil*a females. Genetics 180, 61–72.
Zhang, Y., Chen, D., Wang, Z.H., 2009. Analyses of mental dysfunction-related ACSl4 in *Drosophila* reveal its requirement for Dpp/BMP production and visual wiring in the brain. Hum. Mol. Genet. 18, 3894–3905.
Zhu, S., Wildonger, J., Barshow, S., Younger, S., Huang, Y., Lee, T., 2012. The bHLH repressor Deadpan regulates the self-renewal and specification of *Drosophila* larval neural stem cells independently of Notch. PLoS One 7, e46724.